Asymmetry between the sidebands used for detecting gravitational waves in laser interferometric antennas

Erika D'Ambrosio and Bill Kells

California Institute of Technology, M.C. 18-34, Pasadena, California 91125

Received December 9, 2002; revised manuscript received August 1, 2003; accepted September 29, 2003

We develop an analytical approach in order to understand the causes of sidebands imbalance. The results have been tested by two different and more sophisticated numerical tools. The main static perturbations that can generate sidebands imbalance are described and fully analyzed, with a special attention to the design of the Laser Interferometer Gravitational Wave Observatory I, whose typical parameters have been used for numerical estimations of this phenomenon. © 2004 Optical Society of America

OCIS codes: 140.4780, 040.2840, 290.0290.

1. INTRODUCTION

Several ground-based interferometers have been designed and built in order to detect gravitational waves. The Laser Interferometer Gravitational Wave Observatory (LIGO) consists of two antennas in the United States, and Virgo and GEO are similar projects developed in Europe. A future kilometer-sized interferometer is being planned for construction in Japan, where the prototype TAMA300 is already successfully running. The advanced techniques that are used in those interferometers have been studied and tested for years. In some cases, smaller-scale prototypes have been involved, as the 40-m prototype for LIGO in Pasadena and the 10-m prototype for GEO in Glasgow. The detection schemes may vary and in general involve the use of sidebands. These are generated by modulating the laser light before it enters the Michelson interferometer. Since the effect of a gravitational wave on the electromagnetic field circulating inside the long-arm cavities can be represented as a phase shift, there will be a total of two sets of sidebands: one due to the modulation at frequency f_{mod} and one at the gravitational-wave frequency $f_{\mathrm{gw}} \ll f_{\mathrm{mod}}$. At the operating point, the amount of carrier light exiting through the output port of the interferometer is zero. The only signal detected at the output port is due to the two sets of sidebands. The output power will therefore contain components at $2f_{\mathrm{gw}}$ and $2f_{\mathrm{mod}}$ in addition to the direct-current signal, but the important term is the one obtained by the beat of those at $f_{\mathrm{mod}} \pm f_{\mathrm{gw}}$. This is the only term proportional to the gravitational-wave amplitude. Applying a demodulation at f_{mod} allows the interesting term to be converted at the gravitational-wave frequency f_{gw}. In planning this scheme, known as heterodyne detection, the amplitude of the radio-frequency sidebands is assumed to be identical for the two, but, both in the 40-m prototype and recently in LIGO I, evidence of an imbalance has been found. Because of the high sensitivity that is required for detecting gravitational waves and the technological challenge implied in assembling and working with the best of the current state-of-the-art devices, we tackled this issue in order to investigate the physical mechanisms for which the sidebands do not interact in the same way with the interferometer. The experimental data have shown a difference in the gain of the RF sidebands, with slow fluctations at around 1 Hz. In the model we propose, the sidebands imbalance is static, and this corresponds to the mean imbalance observed at the spectral analyzer. This analytical model is described in Section 3, and it has some features of its own that we will briefly discuss since it is different from the generally used optical modal model. In Section 1, we start with the simple case of one single mode and longitudinal perturbations. The more general case is dealt with in Section 2, which is the core of the paper. In Section 4, we list the distorted configurations that make the sidebands asymmetric, and also we comment on how such an effect can be minimized, although it cannot be entirely eliminated. This is indeed the crucial and original point of the research presented here, besides the analytical tools we develop for studying the problem.

2. SINGLE-MODE SITUATION

Let us start with a variant of the Michelson interferometer: A recycling mirror, whose high-reflective surface is taken as a reference point, is placed between the light source and the beam splitter. The symmetric scheme is illustrated in Fig. 1, and $r_1 = r_2$ for the mirrors at the end of the two branches.

In gravitational-wave interferometers, those mirrors are indeed substituted by long Fabry–Perot cavities that we are not considering for now. The propagation of the two sidebands, back and forth between the end mirrors and the recycling mirror, is represented by

$$P_{\text{round-trip}} \propto \exp[i(k \pm k_{\mathrm{mod}})l_+]\cos[(k \pm k_{\mathrm{mod}})l_-],$$

$$k = \frac{2\pi f_{\mathrm{CR}}}{c} = \frac{2\pi}{\lambda}, \qquad k_{\mathrm{mod}} = \frac{2\pi f_{\mathrm{mod}}}{c} = \frac{2\pi}{\lambda_{\mathrm{mod}}},$$

0740-3224/2004/020233-10$15.00

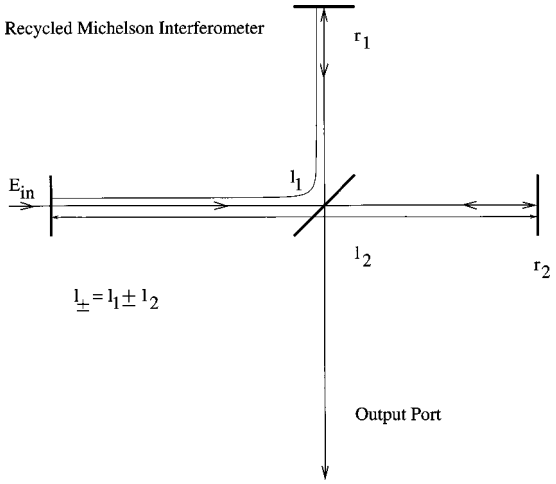

Fig. 1. Laser light enters the cavity through the recycling mirror. There are specific conditions that make the amplitude of the electromagnetic fields identical at the sideband frequencies $f_{CR} \pm f_{mod}$ in the steady state.

with $l_+ = l_1 + l_2$ and $l_- = l_1 - l_2$ defined in Fig. 1. The standard conditions for the carrier,

$$kl_+ = n\pi, \qquad kl_- = m\pi, \qquad m,n \in \mathcal{I},$$

make the sidebands symmetrical. If they are not satisfied, the carrier is not resonating, and it is leaking out of the antisymmetric port. Because of those deviations,

$$\delta l_+,\ \delta l_- \neq 0 \Rightarrow P_{\text{round-trip}} \propto \exp[i(k\,\delta l_+ \pm k_{\text{mod}} l_+)]\cos(k\,\delta l_- \pm k_{\text{mod}} l_-)$$

is the round-trip propagation of the sidebands, and the peak amplitude for one of the two is increased, while it decreases for the other. In order to have the same sidebands amplitude for any δl_- and δl_+, the conditions

$$\exp(ik_{\text{mod}} l_+) = \pm 1, \qquad \exp(ik_{\text{mod}} l_-) = \pm 1,$$

should be satisfied; otherwise, the resonant curves of the sidebands are peaked on different values of δl_+. This effect can be compensated by locking the common length on the laser frequency or adjusting f_{mod}. The distances between mirrors have been designed in LIGO in such a way that the macroscopic length l_+ is an integer multiple of $\lambda_{\text{mod}}/2$. Since l_- is not a multiple of $\lambda_{\text{mod}}/2$, the microscopic condition $\delta l_- = 0$ has to be satisfied in order to have the resonant curves of the sidebands equivalent.

If $\delta l_- \neq 0$, the amount of light at the dark port is not the same for the two sidebands, and therefore the maximum power that can be recycled is not the same, despite the fact they can both be at their peak value for the proper macroscopic and microscopic conditions on l_+, corresponding to simultaneous resonance of the sidebands. For the case $r_1 = r_2$, the effect of those conditions on the amplitude of the sidebands is better visualized in Fig. 2. Then we can introduce some frequency-independent imperfections that break the symmetry of the Michelson interferometer we are studying.

For example, the propagator

$$\exp[i(k \pm k_{\text{mod}})l_+]\left\{\frac{r_1 + r_2}{2}\cos[(k \pm k_{\text{mod}})l_-] + i\,\frac{r_1 - r_2}{2}\sin[(k \pm k_{\text{mod}})l_-]\right\}$$

corresponds to a configuration where the reflectivities $r_1 \neq r_2$ for the two end mirrors are different. In this case, $\delta l_- = 0$ is the right choice for minimizing the amount of carrier light at the output port. When the common length is properly tuned so that $\delta l_+ = 0$, the sidebands are balanced. In all other cases, they are not. The sideband fields gain a different phase shift when they propagate through the recycled Michelson interferometer, so that, for a full round trip,

$$P_{\text{round-trip}} \propto \exp\left[i(k\,\delta l_+ \pm k_{\text{mod}} l_+) \pm i \arctan\frac{(r_1 - r_2)\sin k_{\text{mod}} l_-}{(r_1 + r_2)\cos k_{\text{mod}} l_-}\right],$$

and the modulation frequency ought to be changed, in order to match the varied macroscopic condition on k_{mod}. The overall design is such that the fields are very sensitive to any asymmetry between the arms of the interferometer. We will see that a typical asymmetry is related to the radii of curvature; they might be different for imperfections of their own, but more likely the mirrors are exposed to different power loads, and they are influenced by different thermal distortions. Even if the power loads were exactly the same, the arms of the interferometer would still be different because of the beam splitter. When the optical path length through the bulk of the beam splitter is distorted in a nonuniform way, the geometrical symmetry between the two arms is broken, and it cannot be recovered simply by adjusting δl_+ and δl_-. This is due to a different interaction of the transverse degrees of freedom of the electromagnetic field with the optics in the two branches, and the single-mode treatment is not suitable for analyzing the consequences of such an asymmetry.

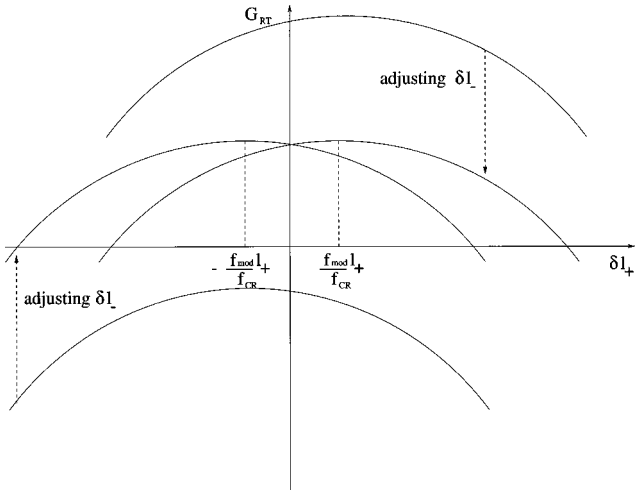

Fig. 2. Power gain at the beam-splitter symmetric port G_{RT} is simply defined as a function of two longitudinal quantities: $f_{CR}\delta l_- \pm f_{mod} l_-$, which corresponds to a differential phase, and $f_{CR}\delta l_+ \pm f_{mod} l_+$, which corresponds to a common phase for the sidebands at $f = f_{CR} \pm f_{mod}$.

3. GENERAL DISTORTED CONFIGURATIONS

In the previous section, we have treated only one degree of freedom, neglecting the transverse distribution of the electromagnetic field. If the dependance on the transverse degrees of freedom is included, besides microscopic adjustments of the lengths, the modal content of the input field can be optimized in order to reduce sidebands asymmetry.

First, we consider a symmetric configuration with exactly the same branches. For this purpose, we assume that the beam splitter is perfect so that there is no difference in the modal content of the beams traveling on l_1 and l_2.

We also use a radio-frequency modulation with $f_{\mathrm{mod}} \ll f_{\mathrm{CR}}$ so that sidebands and carrier can be expanded with the same set of modes. This allows us to express the perturbation operators by the same matrices for carrier and sidebands. This approximation also implies that perturbation operators are not frequency dependent. For this reason, we do not include the Fabry–Perot arms yet, restricting our attention to the central area of the interferometer whose length $l_+/2$ is relatively short compared with the typical distance the field has to travel before it experiences a significant variation in its transverse distribution. For example, in LIGO, the spot size is nearly constant, ~3.6 cm, throughout the recycling cavity.

If all the above assumptions are satisfied, for any symmetric configuration of the Michelson interferometer, the sidebands are balanced. We can generalize the previous argument about the different reflectivities of the end mirrors, using the corresponding *modified* formula,

$$\exp[i(k \pm k_{\mathrm{mod}})l_+]p\left\{\frac{m_1 + m_2}{2}\cos[(k \pm k_{\mathrm{mod}})l_-] + i\frac{m_1 - m_2}{2}\sin[(k \pm k_{\mathrm{mod}})l_-]\right\}p,$$

where the scalars r_1 and r_2 have been replaced by the matrices m_1 and m_2. The transverse propagator p that we introduced takes into account the different phases acquired by the optical modes of the cavity, when they travel from the recycling mirror to the end mirrors. The differential length l_- is supposed to have no effect other than a purely longitudinal delay so that the same basis and the same matrix p is used for the two branches. For $m_1 = m_2$, the sidebands are balanced.

There is another interesting configuration that ensures sidebands balance: if the perturbations in the two branches are equal and opposite. In this case, the electromagnetic field in the two branches will be perturbed in a differential way. Because of this, the components generated by the perturbation will exactly cancel each other at the symmetric port of the beam splitter. At the same time, the content of the light leaking out of the interferometer at the output port totally consists of the excited mode due to the scattering. The formalism we chose in order to model this phenomenon is illustrated in the next section.

The common mode circulating in the recycling cavity and the excited mode that exits through the dark port form a basis of eigenmodes of the cavity. There is a special configuration that helps in simplifying things: if the output fields and the input fields are selected at the same distance from the beam splitter.

This allows us to use the same propagator p for the phase transformation of the transverse modes. The output fields are thus obtained from the circulating field, by the operator

$$\exp[i(k \pm k_{\mathrm{mod}})l_+]p\left\{i\frac{m_1 + m_2}{2}\sin[(k \pm k_{\mathrm{mod}})l_-] + \frac{m_1 - m_2}{2}\cos[(k \pm k_{\mathrm{mod}})l_-]\right\}p, \quad (1)$$

standing for the propagation from the recycling mirror to the two end mirrors and back through the antisymmetric port of the beam splitter, exiting the dark port. If the eigenmode v_1 is chosen as the input beam, it follows that the power at the output will be in the form v_2. Conversely, if v_2 is the input field, v_1 will be the output. This behavior of the differential configuration may be better envisioned by applying a time-reversal transformation, so that v_1 enters the interferometer from the output port, and, because of the geometrical properties of this configuration, v_2 is generated and propagated toward the recycling mirror (and vice versa).

The sidebands are balanced: We assume that they are represented by the same input field as the carrier, as they are generated by phase modulation and pass through the same mode cleaner.[1]

Therefore the input beam for the sidebands is the same as for the carrier, and it corresponds to the resonating mode for the symmetrical configuration. Since m_1 and m_2 are not diagonal, the total round-trip operator has completely different features for the carrier and the sidebands. As an example, we analyze the case of misalignment:

$$p = \begin{bmatrix} \exp(i\theta_G) & 0 \\ 0 & \exp(2i\theta_G) \end{bmatrix},$$

$$m_1 = \begin{bmatrix} \sqrt{1-\epsilon^2} & i\epsilon \\ i\epsilon & \sqrt{1-\epsilon^2} \end{bmatrix},$$

$$m_2 = \begin{bmatrix} \sqrt{1-\epsilon^2} & -i\epsilon \\ -i\epsilon & \sqrt{1-\epsilon^2} \end{bmatrix},$$

in the *unperturbed* basis.

Using the complete and orthonormal set of Hermite–Gauss eigenmodes, we find that θ_G is the Guoy phase and $\epsilon = \sin(kw\theta_{\mathrm{tilt}})$, with $k = 2\pi f_{\mathrm{CR}}/c$ and w the spot size. We find that for this differential perturbation, the set of carrier eigenmodes is[2]

$$v_1 = \begin{pmatrix} 1 \\ \dfrac{-i\sin(k\,\delta l_-)}{2\cos(k\,\delta l_-)\sin\theta_G}\epsilon \end{pmatrix},$$

$$v_2 = \begin{pmatrix} \dfrac{i\sin(k\,\delta l_-)}{2\cos(k\,\delta l_-)\sin\theta_G}\epsilon \\ 1 \end{pmatrix},$$

corresponding to the eigenvalues

$$\lambda_1 = \sqrt{\cos^2(k\,\delta l_-) - \epsilon^2} \times \exp\left[2i\,\theta_G + i\,\frac{\epsilon^2 \tan^2 k\,\delta l_-}{2\tan\theta_G}\right] \times \exp[i(k\,\delta l_+ \pm k_{\mathrm{mod}} l_+)],$$

$$\lambda_2 = \sqrt{\cos^2(k\,\delta l_-) - \epsilon^2} \times \exp\left[4i\,\theta_G - i\,\frac{\epsilon^2 \tan^2 k\,\delta l_-}{2\tan\theta_G}\right] \times \exp[i(k\,\delta l_+ \pm k_{\mathrm{mod}} l_+)],$$

while for the sidebands

$$v_1^{\pm} = \begin{pmatrix} 1 \\ \dfrac{-i\sin(k\,\delta l_- \pm k_{\mathrm{mod}} l_-)}{2\cos(k\,\delta l_- \pm k_{\mathrm{mod}} l_-)\sin\theta_G}\epsilon \end{pmatrix},$$

$$v_2^{\pm} = \begin{pmatrix} \dfrac{i\sin(k\,\delta l_- \pm k_{\mathrm{mod}} l_-)}{2\cos(k\,\delta l_- \pm k_{\mathrm{mod}} l_-)\sin\theta_G}\epsilon \\ 1 \end{pmatrix}, \tag{2}$$

corresponding to the eigenvalues

$$\lambda_1^{\pm} = \sqrt{\cos^2(k\,\delta l_- \pm k_{\mathrm{mod}} l_-) - \epsilon^2} \times \exp\left[2i\,\theta_G + i\,\frac{\epsilon^2 \tan^2(k\,\delta l_- \pm k_{\mathrm{mod}} l_-)}{2\tan\theta_G}\right] \times \exp[i(k\,\delta l_+ \pm k_{\mathrm{mod}} l_+)],$$

$$\lambda_2^{\pm} = \sqrt{\cos^2(k\,\delta l_- \pm k_{\mathrm{mod}} l_-) - \epsilon^2} \times \exp\left[4i\,\theta_G - i\,\frac{\epsilon^2 \tan^2(k\,\delta l_- \pm k_{\mathrm{mod}} l_-)}{2\tan\theta_G}\right] \times \exp[i(k\,\delta l_+ \pm k_{\mathrm{mod}} l_+)],$$

where calculations have been done up to $\mathcal{O}(\epsilon^2)$. For example if v_1 is fed into the interferometer, the field exiting the dark port would be

$$v_{\mathrm{OUT}} = \begin{pmatrix} -i\sin(k\,\delta l_-)\exp\left[-i\,\theta_G - \dfrac{i\epsilon^2}{2\tan\theta_G}\right] \\ \dfrac{1}{2\cos(k\,\delta l_-)}\left[\dfrac{\sin^2 k\,\delta l_-}{\tan\theta_G} + i(1+\cos^2 k\,\delta l_-)\right]\epsilon \end{pmatrix} \times \exp(3i\,\theta_G + ikl_+), \tag{3}$$

obtained by applying the operator (1). The antisymmetric port of the beam splitter ought to be set so that $|\lambda_1|$ is maximum. This condition corresponds to $\delta l_- = 0$, and for this choice $v_{\mathrm{OUT}} \propto v_2$. At the same time, $v_1^+ = v_1^{-*}$. Similar considerations to the ones we have done for the one-dimensional case can be applied here for one eigenmode. After one is selected, the longitudinal degrees of freedom must be tuned accordingly.

The modal content of the carrier and sideband eigenmodes would be the same if $l_- = 0$, as we can see from Eqs. (2). Due to the differential perturbation, the mode mixing for the sidebands depends on the Schnupp asymmetry. It follows that, when the system is driven by v_1, the sideband eigenmodes $v_1^{\pm}$ and $v_2^{\pm}$ are both excited. However, for small perturbations and if the system is nondegenerate, the modes $v_2^{\pm}$ are basically suppressed, and the optical modes $v_1^{\pm}$ are equally close to resonance. Their coupling with v_1 is the same for $\delta l_- = 0$, and the power gain is also the same.

4. UNITARY MODAL MODEL

The considerations we have done for the one-dimensional case apply in general when the end mirrors are equivalent because of the geometry of the system. The symmetry is broken only if the end mirrors are different and therefore we are interested in *differential* perturbations.

Motivated by this, we developed a model satisfying the following requirements:

1. Since we want to deal with scattering matrices that are not frequency dependent, the Fabry–Perot cavities are not included yet.
2. We also deal with one distortion at a time, while for more general perturbations, sophisticated numerical tools are needed beyond a simple 2×2 model.
3. The perturbations we aim to model are geometrical distortions of mirrors with no loss of energy so that time-reversal properties are easy to interpret.[3]

We included all these requirements in a model based on unitary matrices. Since we consider one kind of perturbation, m_1 and m_2 have the same functional form that will depend on the size of the distortion. We are also looking for a functional form that manifestly allows the operator to be split, since we want to make use of the geometrical properties of the symmetric and antisymmetric interferometer. These requirements are satisfied by a model based on the Pauli operators. For example, in Fig. 3, the reflection upon the end mirrors is represented by the matrices $m_1 = m(a)$ and $m_2 = m(b)$. Using the generators of SU(2), we can split them as in $m(a) = m[(a+b)/2]m[(a-b)/2]$. If the perturbation is due to misaligned mirrors, $m(a) = \exp(ia\sigma_x)$. The general form would be $\exp(ia\mathbf{n}\cdot\boldsymbol{\sigma})$. For example, if the perturbation consists of a mismatch of the curvature of the mirrors, the Guoy phases of the cavity modes are affected at the first order in the distortion. This basically corresponds to a modification of the vacuum propagator p. At the first order,

$$\delta p = \begin{bmatrix} i\exp(i\,\theta_G)\dfrac{\mathrm{d}\theta_G}{\mathrm{d}R}\Delta R & 0 \\ 0 & 3i\exp(3i\,\theta_G)\dfrac{\mathrm{d}\theta_G}{\mathrm{d}R}\Delta R \end{bmatrix}, \qquad R = \text{radius of curvature}, \tag{4}$$

corresponds to the variation of the phases the unperturbed modes acquire, when they travel from the recycling mirror to one of the two end mirrors. There are two optical paths represented by l_1 and l_2, each of which is affected in a different way if ΔR is not the same in the two mirrors. At the first order, we can write

$$m_1 = \exp(i\,\alpha)\begin{bmatrix} \exp(-i\beta)\cos\gamma & i\sin\gamma \\ i\sin\gamma & \exp(i\beta)\cos\gamma \end{bmatrix},$$

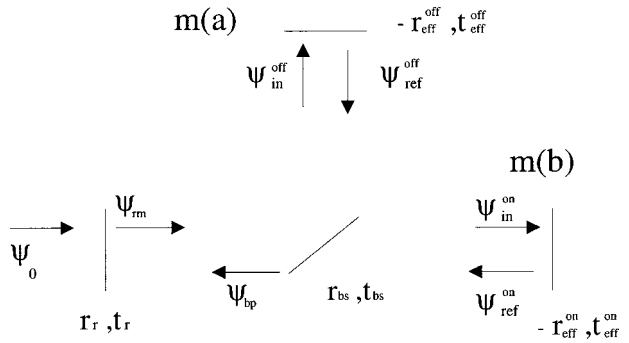

Fig. 3. Scattering among the cavity modes is represented by the operators $m(a)$ and $m(b)$. In the frequency-independent case, they are unitary matrices that depend on some adimensional parameter, proportional to the distortion, as for tilt or curvature mismatch. In the 2×2 model we have constructed, we generated the unitary matrices from the Pauli matrices, overriding the usual modal-model rules.

which is both unitary and symmetric. Similarly we can express m_2 and for the variation in the radius of curvature, $\gamma = \beta = \alpha/2$. We have included the variation corresponding to Eq. (4) in m_1 so that the formula for the round-trip propagation can be written in the same form we have used above,

$$\exp[i(k\delta l_+ \pm k_{\mathrm{mod}} l_+)]p\left[\frac{m_1 + m_2}{2}\cos(k\delta l_- \pm k_{\mathrm{mod}} l_-) + i\frac{m_1 - m_2}{2}\sin(k\delta l_- \pm k_{\mathrm{mod}} l_-)\right]p,$$

with unperturbed p. The unitary transformation induced by a variation of the radius of curvature is

$$m_1 = m(a) = \exp(i\sqrt{2}a)\exp(ia\mathbf{n}\cdot\boldsymbol{\sigma}),$$

$$\mathbf{n}\cdot\boldsymbol{\sigma} = \sigma_H = \frac{1}{\sqrt{2}}\begin{bmatrix} -1 & 1 \\ 1 & 1 \end{bmatrix},$$

with σ_H an Hadamard operator and $a = kw^2\Delta R/(\sqrt{2}R^2)$, where $k = 2\pi f_{\mathrm{CR}}/c$ and w is the spot size on the mirror. We have examined the perturbation in the radius of curvature and in the mirror orientation because these are the simplest and most representative examples of a variety of cases.

When the reflective surface of a mirror whose height is $h(x, y)$ does not match the phase front $\phi(x, y)$ of the impinging beam, the difference between them along the direction of propagation,

$$h(x, y) - \frac{\lambda}{2\pi}\Phi(x, y),$$

is a polynomial that we can expand in terms of Hermite functions. The simplest case we can study,

$$h(x, y) - \frac{\lambda}{2\pi}\Phi(x, y) = \frac{\lambda}{4\pi}H_m\left(\frac{\sqrt{2}x}{w}\right)H_n\left(\frac{\sqrt{2}y}{w}\right)\frac{\gamma}{2^{m+n}m!n!}, \quad (5)$$

has the following properties:

$$\langle u_{mn}|m|u_{00}\rangle = i\gamma - \frac{\gamma}{2}2\beta,$$

$$\langle u_{00}|m|u_{00}\rangle = 1 - \frac{\gamma^2}{2},$$

$$\langle u_{mn}|m|u_{mn}\rangle = 1 + i2\beta + \mathcal{O}(\gamma^2),$$

where the scattering matrix

$$m = \exp\left\{2ik\left[h(x, y) - \frac{\lambda}{2\pi}\Phi(x, y)\right]\right\}$$

has been expanded as

$$m = 1 + 2ik\left[h(x, y) - \frac{\lambda}{2\pi}\Phi(x, y)\right] + \frac{1}{2}\left\{2ik\left[h(x, y) - \frac{\lambda}{2\pi}\Phi(x, y)\right]\right\}^2 + \ldots,$$

and we have defined

$$\langle u_{mn}|2k\left[h(x, y) - \frac{\lambda}{2\pi}\Phi(x, y)\right]|u_{mn}\rangle = 2\beta \propto \gamma, \quad (6)$$

with u_{mn} the Hermite–Gauss functions fully described in Subsection 4.B.

Perturbations that are odd in x or y are represented by $\beta = 0$. If the perturbation is even in both x and y, there are terms $\sim\gamma$ also on the diagonal of m. Since we are interested in small perturbations, we can use

$$m \simeq \exp(i\beta) \times \begin{bmatrix} \left(1 - \frac{\gamma^2}{2}\right)\exp(-i\beta) & i\gamma \\ i\gamma & [1 - \mathcal{O}(\gamma^2)]\exp(i\beta) \end{bmatrix}$$

and focus on the eigenmode that is closest to u_{00}. When we do so there is no need to know explicitly the term $\mathcal{O}(\gamma^2)$ in m above. In fact, that would always be multipled by a quantity that is of the order of γ.

In Fig. 4, we have reported the common and differential perturbation cases for the radius of curvature. For any situation that is not $m_1 = m_2$, the differential phase needs to be adjusted. The optimal choice corresponds to the maximum absolute value of the eigenvalue: This

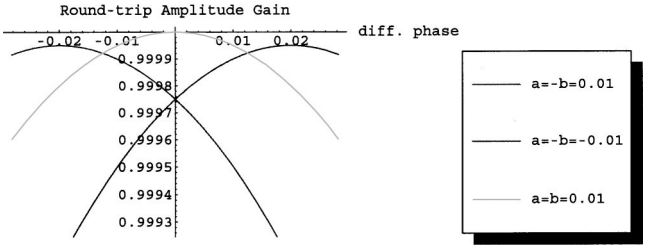

Fig. 4. Peak of the field amplitude after one round trip corresponds to a different position of the beam splitter than in the unperturbed case. The same microscopic tuning that maximizes such amplitude for one eigenmode makes dark the output port for that specific eigenmode. Here a and b are proportional to a change in the radius of curvature. Using the LIGO typical values $a = 0.01$ corresponds to a variation of the thank you order of $\Delta R \sim 400$ m over $R = 14571$ m.

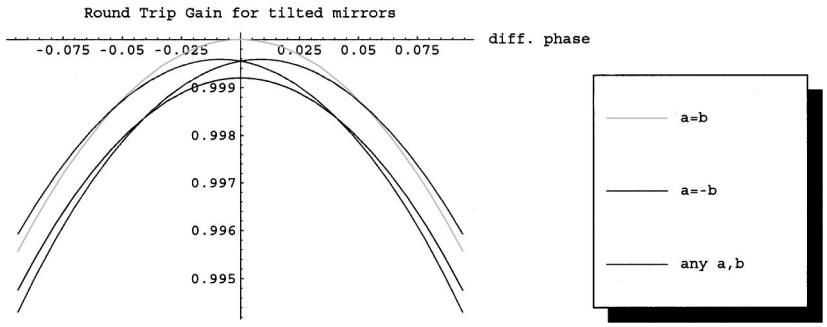

Fig. 5. When the optical axes of the two branches are misaligned, the position of the beam splitter must be tuned in order to make all the light that is associated with the resonating mode recycled. The same tuning is the one that ensures there is no resonating mode at the output port and restores a symmetric interaction of the sidebands with the interferometer, provided the driving beam is matched with the resonating eigenvector.

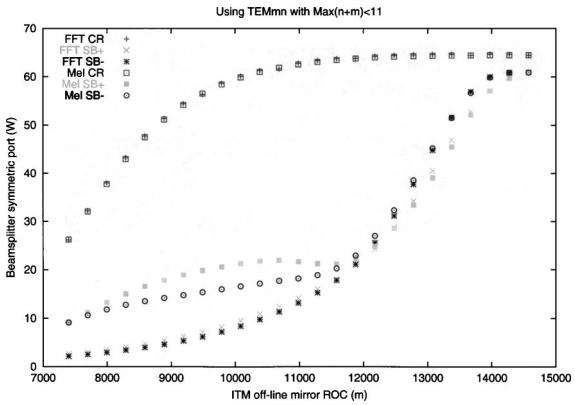

Fig. 6. Power stored in the recycling cavity when one of the two branches is perturbed because of a curvature mismatch. The design value is 14571 m, and the relative sidebands imbalance is ~20% in the range 13000–13500 m.

guarantees that the output port is dark for the resonating mode and the maximum amount of power gets recycled.

We can see similar properties in Fig. 5 when the mirrors are tilted by any amount. As the differential phase for the sidebands is $\pm k_{\mathrm{mod}} l_-$ around the value corresponding to the maximum (which is the best choice for the carrier), the power associated with the sidebands will be almost the same since the curve is approximately parabolic near its maximum. The equivalence is true only through second order.

From a quantitative point of view, the situation becomes complicated when many modes are involved, although the concepts we have outlined in our analysis are still valid. In Fig. 6, the power circulating in the recycling cavity is shown for the carrier and the two sidebands, as a function of the radius of curvature of one mirror.

Two numerical programs have been used: One is a fast-Fourier-transform model, which make the representation of the electromagnetic field switch back and forth between the space and the frequency domain; the other is a MATLAB code based on a large subset of the Hermite–Gauss basis. Although for the carrier the two approaches give the same results, corresponding to the two curves on the top part of the graph that are practically the same, when R is far below the ideal value 14571 m, there is a large inconsistency between the values obtained by the two programs for the sidebands. However, for distortions

$$|\Delta R| \leqslant 2500 \text{ m} \Rightarrow |a| = \left| \frac{k w^2}{2} \left(\frac{1}{R_{\mathrm{pert}}} - \frac{1}{R_{\mathrm{design}}} \right) \right| \leqslant 0.05, \qquad |b| = 0,$$

$$w = 3.6 \text{ cm}, \qquad k = \frac{2\pi f_{\mathrm{CR}}}{c} = \frac{2\pi}{\lambda},$$

$$\lambda = 1.064\, 10^{-6} \text{ m},$$

the agreement between the values obtained by the two codes is remarkably good.

5. BEYOND THE FREQUENCY-INDEPENDENT MODEL

We have not yet tackled the full interferometer configuration, with additional Fabry–Perot cavities, where only the carrier is resonating. This means that the total reflection from the arms is not simply a general scattering but depends on the frequency of the electromagnetic field. In order to extend our model to more complex situations when the arms are included, we start investigating the effects of macroscopic and microscopic mistuning on the electromagnetic field, when this is represented by one degree of freedom only. We include in the very formula we used for the recycled Michelson interferometer $r_i = r_i(f)$. Taking the end mirrors perfectly reflective and assuming for the input mirror of the Fabry–Perot the same reflectivity for its reflective and anti-reflective side,

$$r_1(f) = \frac{-r_1 + \exp(2\pi i f 2L_1/c)}{1 - r_1 \exp(2\pi i f 2L_1/c)}, \qquad |r_1(f)| = 1,$$

$$r_2(f) = \frac{-r_2 + \exp(2\pi i f L_2/c)}{1 - r_2 \exp(2\pi i f L_2/c)}, \qquad |r_2(f)| = 1,$$

so that we can write the total round-trip propagation, for the central part of the interferometer, as an extension of the unidimensional formula we have used for the recycling cavity

$$\exp[i(k\,\delta l_+ \pm k_{\mathrm{mod}} l_+)] \times \left\{ \frac{r_1(f_{\mathrm{CR}} \pm f_{\mathrm{mod}}) + r_2(f_{\mathrm{CR}} \pm f_{\mathrm{mod}})}{2} \cos(k\,\delta l_- \pm k_{\mathrm{mod}} l_-) + i\,\frac{r_1(f_{\mathrm{CR}} \pm f_{\mathrm{mod}}) - r_2(f_{\mathrm{CR}} \pm f_{\mathrm{mod}})}{2} \sin(k\,\delta l_- \pm k_{\mathrm{mod}} l_-) \right\},$$

where we can insert

$$r_1(f_{\mathrm{CR}} \pm f_{\mathrm{mod}}) = \exp\left\{ i \arctan \frac{(1 - r_1^2)\sin[2(k \pm k_{\mathrm{mod}})L_1]}{(1 + r_1^2)\cos[2(k \pm k_{\mathrm{mod}})L_1] - 2r_1} \right\}, \tag{7}$$

$$r_2(f_{\mathrm{CR}} \pm f_{\mathrm{mod}}) = \exp\left\{ i \arctan \frac{(1 - r_2^2)\sin[2(k \pm k_{\mathrm{mod}})L_2]}{(1 + r_2^2)\cos[2(k \pm k_{\mathrm{mod}})L_2] - 2r_2} \right\}, \tag{8}$$

as the *effective reflectivities*.

The same considerations we have been doing for the central interferometer can be stated again for the Michelson with Fabry–Perot arms, with real reflectivities

$$\sin[2(k \pm k_{\mathrm{mod}})L_1] = \sin[2(k \pm k_{\mathrm{mod}})L_2] = 0,$$

corresponding to the working point of the gravitational-wave antenna. When the macroscopic condition is satisfied,

$$\cos(2k_{\mathrm{mod}}L_1) = \cos(2k_{\mathrm{mod}}L_2) = -1,$$

and we can compensate for

$$r_1(f_{\mathrm{CR}} \pm f_{\mathrm{mod}}) \simeq -\exp\left(i\,\frac{1 - r_1}{1 + r_1} 2k\,\delta L_1 \right), \tag{9}$$

$$r_2(f_{\mathrm{CR}} \pm f_{\mathrm{mod}}) \simeq -\exp\left(i\,\frac{1 - r_2}{1 + r_2} 2k\,\delta L_2 \right), \tag{10}$$

simply by adjusting δl_-, since Eqs. (9) and (10) do not depend on f_{mod}, and any asymmetry between the sidebands is canceled when

$$\exp(ik_{\mathrm{mod}} l_+) = -1;$$

otherwise, the microscopic condition

$$\exp\left[ik \left(\delta l_+ + \frac{1 - r_1}{1 + r_1}\delta L_1 + \frac{1 - r_2}{1 + r_2}\delta L_2 \right) \right] = 1 \tag{11}$$

must be fulfilled. Note that these conditions are different from the ones that are equivalent to set the antisymmetric port of the beam splitter on the dark fringe of the carrier.

In fact, from Eqs. (7) and (8), we can derive the reflectivities

$$r_1(f_{\mathrm{CR}}) \simeq \exp\left(i\,\frac{1 + r_1}{1 - r_1} 2k\,\delta L_1 / c \right), \tag{12}$$

$$r_2(f_{\mathrm{CR}}) \simeq \exp\left(i\,\frac{1 + r_2}{1 - r_2} 2k\,\delta L_2 / c \right), \tag{13}$$

which result in a differential phase, that should be compensated for by tuning

$$\delta l_- + \frac{1 + r_1}{1 - r_1}\delta L_1 - \frac{1 + r_2}{1 - r_2}\delta L_2 = 0$$

in order to prevent any carrier light from exiting through the output port of the interferometer. We can use a similar argument for Eq. (11) that is not equivalent to lock δl_+ on the resonant condition for the carrier.

This typical behavior has been known for a long time, since it was first seen in the results of the numerical simulations: achieving the same power gain for the two sidebands was always possible by moving the beam splitter. Nonetheless, this spoils the "contrast."[4]

We will use a rather peculiar case in order to better explain this phenomenon. Let us assume that everything is symmetric so that $L_1 = L_2$ and $r_1 = r_2$. The two arms are equally detuned so that $\delta L_1 = \delta L_2$. We can write the equation for the reflectivities

$$r(f_{\mathrm{CR}} \pm f_{\mathrm{mod}}) = \exp\left[i \arctan \frac{(1 - r^2)\sin(\pm 2k_{\mathrm{mod}}L)}{(1 + r^2)\cos(\pm 2k_{\mathrm{mod}}L) - 2r} \right] \times \exp\left[i\,\frac{(1 - r^2)2k\,\delta L}{1 + r^2 - 2r\cos[\pm 2k_{\mathrm{mod}}L)} \right]$$

as a function of r, L, and δL for $\cos(\pm 2k_{\mathrm{mod}}L) \neq -1$. Then we insert the above expression in the round-trip propagator: The configuration is perfectly symmetric, but the round-trip phase in the recycling cavity shows a difference for $f_{\mathrm{CR}} \pm f_{\mathrm{mod}}$. Because of this structural asymmetry, the power stored in the recycling cavity is not the same for the two sidebands. In Fig. 7, the power at the bright port of the beam splitter is plotted versus δL for both the sidebands. The effective reflectivities for the carrier (12) and (13) are compensated for by the choice

$$\delta l_+ + 2\,\frac{1 + r}{1 - r}\delta L = 0,$$

but in order to achieve a symmetric operating point for the two sidebands, the modulation frequency f_{mod} must be adjusted. When the general case of more than one cavity

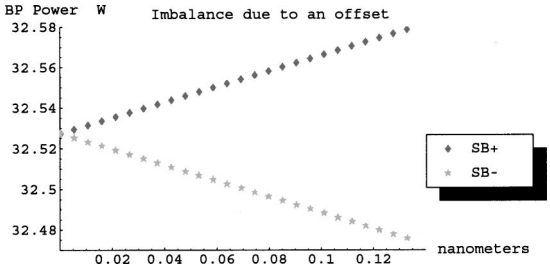

Fig. 7. Example of a frequency-dependent perturbation whose result is a different bright-port power for the two sidebands. The physical mechanism is purely longitudinal: The Fabry–Perot cavities are identical and affected by the same offset, plus the condition $L = (2n + 1)\lambda_{\mathrm{mod}}/4$ is not satisfied.

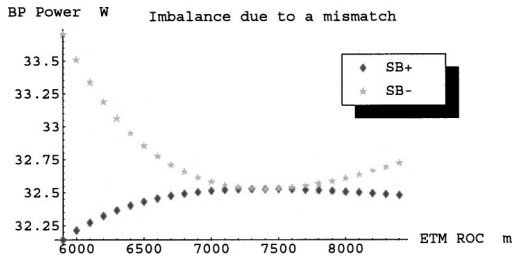

Fig. 8. If the coupling between the recycling and the Fabry–Perot cavities is not exactly matched, the power stored by the two sidebands may be different if the macroscopic condition $L = (2n + 1)\lambda_{mod}/4$ is not fulfilled. There is no geometrical asymmetry between the two arms, but the frequency dependance of the arm reflectivities gives rise to a different interaction of the sidebands with the perturbed interferometer.

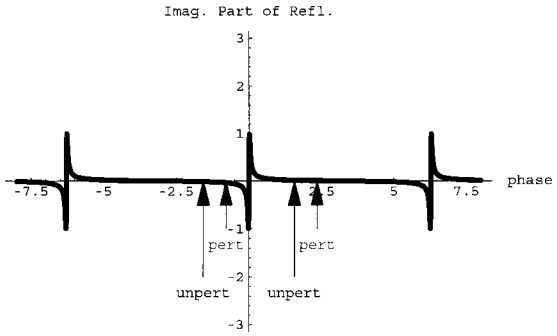

Fig. 9. If the absolute value of the arm reflectivity is one, we can limit our attention to its imaginary part, which is a function of the phase gained after a full round trip inside the Fabry–Perot cavity. The two sidebands are located symmetrically around the carrier whose round-trip phase is zero by definition. This is not true for the higher-order modes excited by a geometrical mismatch.

mode is addressed, we can use some analogies with the analysis we did for the recycled Michelson interferometer. One of the two eigenmodes of the system is chosen to be the resonating one, and it is assumed to be matched by the laser beam.

For this eigenmode, prescriptions similar to the ones we have been working out in the unidimensional case play the same role in canceling the effect of the geometrical distortions on the symmetry at $\pm f_{mod}$ around f_{CR}. They restore the balance for that eigenmode but not for the other ones, and even if a solution can be found that guarantees the same power gain for the sidebands, the composition of the corresponding eigenmodes is not the same. Since the two sidebands are originated by the same optical mode defined for the carrier, the balance can never be entirely restored but only minimized. For the geometrical distortions that break the symmetry of the interferometers, mechanisms similar to the ones we have analyzed for the recycling cavity are responsible for the excitation of higher-order modes and hence for a different interaction of the sidebands with the interferometer.

In Fig. 8, the power stored in the recycling cavity is shown for the two sidebands versus the radius of curvature of the external test mass mirror. The value that perfectly matches the curvature of the beam, whose spot size on the internal test mass mirror is conditioned by the geometrical parameters of the recycling cavity, is $R_{ETM} = 7400$ m, and for any deviation from that which disturbs the arms, the power stored by the two sidebands becomes different. The peculiarity of this perturbation is that it is equally affecting the two arms.

Formally we can write

$$r(f) = \frac{-r + \exp(2\pi i f 2L/c) p m p}{1 - r \exp(2\pi i f 2L_1/c) p m p},$$

where m is the unitary matrix representing the scattering, due to the change in the radius of curvature, and p contains the phase factors, stored in every propagation by the unperturbed modes.[5]

As we have seen in the purely longitudinal case, the imbalance arises when the macroscopic condition $L = (2n + 1)\lambda_{mod}/4$ is not satisfied, although the interferometer is *perfectly symmetrical*.

In order to illustrate the fundamental mechanism, we refer to Fig. 9, where the imaginary part of the arm reflectivity versus the phase gained in a round trip inside the cavity is shown. When $L = (2n + 1)\lambda_{mod}/4$, there is a separation multiple of 2π between the phases corresponding to each mode, at $f_{CR} + f_{mod}$ and $f_{CR} - f_{mod}$. If the above condition fails, we have to distinguish between the unperturbed and the perturbed case. The interaction of the two sidebands with the interferometer is still identical in the former situation, since the arm reflectivities are complex conjugates of each other, so that they are out of resonance by the same amount in the recycling cavity. For the latter case, the situation is complicated by the fact that other modes are excited in addition to the fundamental one. The reflectivity from the long-arm cavity is equivalent for them to different round-trip phases in the recycling cavity for $f_{CR} + f_{mod}$ and $f_{CR} - f_{mod}$, and this intrinsic asymmetry cannot be corrected for by microscopic adjustments. This is the most important difference between the recycled Michelson interferometer and the configuration with Fabry–Perot cavities according to the LIGO-like design. The operators are different for $f_{CR} \pm f_{mod}$ when the complex coupling with the long-arm cavities is taken into account, and that difference can certainly be minimized but not entirely canceled.

6. CONCLUSIONS

An essential part of the detection scheme in gravitational-wave antennas (like LIGO) is the modulation of the laser light that results in the two first harmonics, named the sidebands, that are engaged as a reference for any induced variation of the distance between the mirrors in the Fabry–Perot cavities. The amplitude of them is always assumed to be the same, when the beam splitter is positioned in such a way that no carrier light is leaking out of the dark port. The limit of this assumption has been the focus of our study. The microscopic conditions that are needed for making the carrier field resonating are equivalent to the optimal ones for the minimization of the sidebands imbalance. Our analysis has been confirmed by two numerical programs that are widely used for simulations in the LIGO Laboratories.[6,7]

In addition to the simple geometrical perturbations, we have analyzed the case of frequency-dependent distortions. The role of the macroscopic and microscopic con-

ditions has been described for both the unidimensional and the multimodal treatment. If the Fabry–Perot arms are affected by any imperfection, the effective reflectivity is perturbed in a way that is strongly frequency dependent. In this case, f_{mod} might need to be optimized too. When more than one mode is taken into account, the number of variables that need to be adjusted increases; the transverse degrees of freedom must also be properly tuned. However, since the eigenmodes are not the same for the two sidebands, any feeding beam will result in a combination of eigenmodes, and by microscopic adjustments, we can only restore a symmetric response for a pair of them at $f_{\mathrm{CR}} \pm f_{\mathrm{mod}}$. These phenomena have been investigated by studying the analytical results obtained by a unitary 2×2 model. Within a few percent, we obtained predictions consistent with the output of the more complex programs we employed.

APPENDIX A: GEOMETRICAL INTERPRETATION

The mechanisms working in the case of frequency-independent perturbations can be more clearly viewed by considering the geometrical features of a resonator and a Michelson interferometer. Figure 10 will serve as an illustration for misalignment. The recycling mirror is assumed to be flat. One of the two end mirrors is tilted so that the geometrical symmetry of the interferometer is corrupted. The input beam can be shifted so that it will impinge on the two end mirrors by the same angle, with respect to the surface. Both l_+ and l_- must be adjusted so that one eigenmode is resonating and the output port is set on a dark fringe of that. In this special configuration, the sidebands are symmetric. In LIGO, the angular perturbations of the optics will be sensed and controlled.[8]

A disturbance that is perhaps more interesting for LIGO is a variation of the radius of curvature from the ideal value. This perturbation has also an effect on the phase of the field, and thus it represents the more general case. We use again a geometrical construction to describe the main characteristics of this kind of distortion. In Fig. 11, two mirrors having different curvature are shown along the direction of propagation z. Their position is determined by their radii of curvature in order to match the wave front of the same beam.

The sidebands do not interact in the same way with the interferometer in this case: The phase shift accrued by the nmth-order Hermite–Gaussian mode is not the same in the two arms because of the change in the radius of curvature. The position of the mirrors can be changed in order to set the output port on the dark fringe of one specific mode, but in doing this, the wave front of the beam will no longer match the curvature of the mirrors. As a consequence, some light is scattered into higher-order modes, for which the dark-fringe condition does not hold, and therefore the amplitude of those modes at $f_{\mathrm{CR}} \pm f_{\mathrm{mod}}$ is not equal. The fundamental difference between this kind of distortion and tilt is that the phase change induced on the electromagnetic field is of the order $\mathcal{O}(\Delta R)$ because of the relation between the shape of the surface of the mirror and the longitudinal degree of freedom for propagation. Moreover, each mode acquires a certain differential phase so that we cannot restore the dark-fringe condition for all of them. On the contrary, when the mirrors at the end of the two branches have the same curvature, the dark-fringe condition for every mode is the same, and provided that, the sidebands behave in an analogous way. A similar argument would apply to the common length because for each mode the resonant condition is different, but since $\exp(ik_{\mathrm{mod}}l_+) = -1$ when the carrier is off resonance, the sidebands are also by the same amount. The similar macroscopic condition $k_{\mathrm{mod}}l_- = n\pi$ is not practical, since it implies the antisymmetric port is on the dark fringe for the sidebands as well as for the carrier. On the contrary, l_- has been chosen in LIGO I to maximize the power transmitted at the output by the sidebands, since they are used to amplify the gravitational signal by being beaten against the carrier at the photodetector.

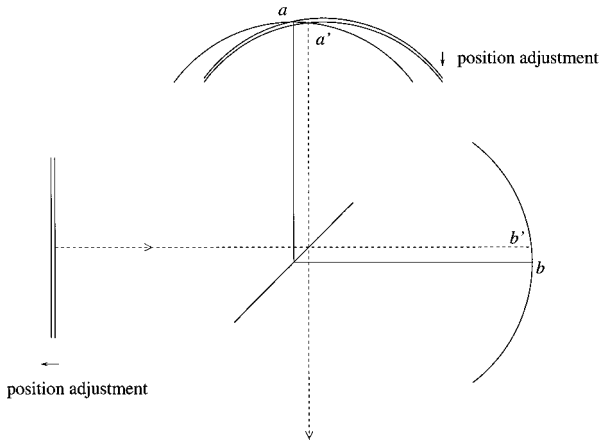

Fig. 10. If the only perturbation is due to misalignment, the mode sustained by the recycled Michelson interferometer is given by a Gaussian beam, whose optic axis is misaligned with respect to the unperturbed cavity axis. The overlap of the electromagnetic fields impinging on the beam splitter, coming from the two branches, is the stable eigenmode, while the remaining part is scattered out of the antisymmetric port and consists of higher-order modes excited by the tilt.

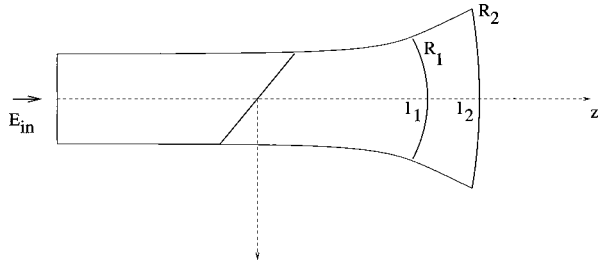

Fig. 11. For small perturbations $l_1 - l_2 \propto R_1 - R_2$ with $l_i = z(R_i)$; as predicted by the paraxial approximation for the propagation of Gaussian beams.

APPENDIX B: HERMITE–GAUSS EIGENMODES

The intensity distribution of laser beams is concentrated along the direction of propagation, and their phase fronts are curved. With fixed waist position and size, the beam dependance on distance is determined by propagation.

The radius of curvature of the wave front is a function of the corresponding intersection with the axis of propagation. The phase shift that is associated with the beam

$$\Phi(z) = kz - (m + n + 1)\arctan\frac{2z}{kw_0^2}$$

is a function of the waist position $z = 0$ and size w_0, and is different for each mode of propagation.

The Hermite–Gauss solutions are

$$u_{mn}(x, y, z) = \sqrt{\frac{2}{\pi w^2(z)}}\exp\left\{-i\Phi(z) - (x^2 + y^2)\times\left[\frac{1}{w^2(z)} + \frac{ik}{2R(z)}\right]\right\} \times \sqrt{\frac{1}{2^{m+n}m!n!}}H_m\left[\frac{\sqrt{2}x}{w(z)}\right]H_n\left[\frac{\sqrt{2}y}{w(z)}\right]$$

and form a complete and orthogonal set of functions. Standard modal models use a finite number of those functions for calculating matrix elements in optical problems. Because of the unitarity that we explicitly required for constructing our model and the geometrical features we wanted to include (in order to split the operators in a common and a differential part), we checked the obtained results by the physical interpretation.

For example, in the case of a misaligned mirror, the fundamental eigenmode that we found corresponds to a Gaussian beam whose axis is shifted so that the two mirrors look misaligned by the same amount, from the point of view of the incoming beam. Furthermore the predicted adjustment of the differential length,

$$k\,\delta l_- = \epsilon^2/(4\tan\theta_G), \qquad \epsilon = kw\,\theta_{\text{tilt}},$$

can be easily interpreted,

$$k\,\delta z = kR(1 - \cos\theta_{\text{tilt}}) = 2kR\sin^2\theta_{\text{tilt}}/2,$$

in the simple case of a flat input mirror since $\theta_G = \arctan[kw^2/(2R)]$.

From the last expression for θ_G, we can also infer that any distortion in the radius of curvature will induce a different phase separation $\Phi(z)$ among the modes traversing the two branches, unless the configuration is still symmetric with the end mirrors changed in the same way and by the same amount.

ACKNOWLEDGMENTS

We thank Stanley E. Whitcomb for suggesting the problem that led us into this research project and Ray Beausoleil for discussions of some numerical results.

This paper was supported by the National Science Foundation under cooperative agreement PHY-9210038.

REFERENCES

1. J. B. Camp, H. Yamamoto, and S. E. Whitcomb, "Analysis of light noise in a recycled Michelson interferometer with Fabry–Perot arms," J. Opt. Soc. Am. A **17**, 120–128 (2000).
2. A. E. Siegman, *Lasers* (University Science, Mill Valley, Calif., 1986).
3. A. Kostenbauder, Y. Sun, and A. E. Siegman, "Eigenmode expansions using biorthogonal functions: complex-valued Hermite–Gaussians," J. Opt. Soc. Am. A **14**, 1780–1790 (1997).
4. P. R. Saulson, *Interferometric Gravitational Wave Detectors* (World Scientific, Singapore, 1994).
5. H. Kogelnik and T. Li, "Laser beams and resonators," Appl. Opt. **5**, 1550–1567 (1966).
6. R. Beausoleil, E. Gustafson, M. Fejer, E. D'Ambrosio, B. Kells, and J. Camp, "Model of thermal wave-front distortion in interferometric gravitational-wave detectors. I. Thermal focusing," J. Opt. Soc. Am. B **20**, 1247–1268 (2003).
7. B. Bochner, "Simulating a dual-recycled gravitational wave interferometer with realistically imperfect optics," Gen. Relativ. Grav. **35**, 1029–1057 (2003).
8. P. Fritschel, N. Mavalvala, D. Shoemaker, D. Sigg, M. Zucker, and G. Gonzalez, "Alignment of an interferometric gravitational wave detector," Appl. Opt. **37**, 6734–6747 (1998).